Microchimica Acta (2023) 190:348
https://doi.org/10.1007/s00604-023-05930-9

ORIGINAL PAPER

Methylene blue molecularly imprinted polymer for melatonin determination in urine and saliva samples

Pachanuporn Sunon[1,2] · **Kamonwad Ngamchuea**[1]

Received: 13 April 2023 / Accepted: 25 July 2023 / Published online: 11 August 2023

Abstract

A highly sensitive and rapid electrochemical sensor was developed for detecting melatonin using a molecularly imprinted polymer (MIP) with methylene blue as the functional monomer and melatonin as the template. The MIP was synthesized via a simple electropolymerization process that did not require an initiating reagent. The sensor demonstrated good selectivity for melatonin against common interferences such as lactate, cytosine, cytidine, urea, ascorbic acid, creatine, creatinine, serotonin, and tryptophan. Melatonin detection was achieved at a potential of 0.60 V vs. Ag/AgCl with a sensitivity of 138.8 ± 4.7 μA μM^{-1} in the linear range 0.097 – 200 μM and a limit of detection of 29 nM ($3S_B/m$). The sensor exhibited excellent reproducibility and repeatability for both within (intra) and between (inter) electrodes (%RSD < 3% for $n = 3$). The sensor was applied to authentic urine and saliva samples with recoveries of $103 \pm 1\%$ and $102 \pm 1\%$, respectively.

Keywords Molecularly imprinted polymer · Melatonin · Biomarker · Methylene blue · Voltammetry

Introduction

Melatonin (*N*-acetyl-5-methoxytryptamine) is a hormone produced by the pineal gland in the brain, primarily in response to darkness. It regulates sleep–wake cycles and plays a crucial role in the body's internal clock [1]. It has various functions, including controlling seasonal rhythms [2], enhancing immune function [3], regulating retinal physiology [4], managing neural stem cells [5], and preventing tumorigenesis [6]. Melatonin acts as an antioxidant, protecting cells from oxidative damage [7]. It may also have a role in mood regulation [8] and can be used to treat jet lag [9], sleep disorders [10], neurodegenerative conditions [11, 12], and has potential anticancer properties [13]. Given the broad spectrum of melatonin's effects on the body, it is crucial to be able to accurately and non-invasively measure melatonin levels.

At present, melatonin can be detected by various techniques such as high performance liquid chromatography-mass spectrometry [14, 15], gas chromatography-mass spectrometry [16], fluorescence [17], spectrophotometry [18, 19], optical sensing [20], capillary electrophoresis with electrochemical detection [21], capillary electrophoresis with UV and fluorometric detection [22], radioimmunoassay [23], enzyme-linked immunoassay (ELISAs) [24, 25], and electrochemical techniques such as voltammetry, amperometry and electrochemical impedance spectroscopy [26, 27]. Among these techniques, electrochemical detection has emerged as one of the most promising due to its low cost, simplicity, ease of operation, robustness, fast measurement, high sensitivity, wide dynamic range, portability, and potential for miniaturization and integration into wearable devices for in vivo and real-time monitoring.

However, the electrochemical detection of melatonin faces several challenges in the development of selective sensors that are not influenced by the matrix and interferences. Electrode fouling by biological components in clinical samples such as blood, saliva, sweat, and urine is another significant challenge in the development of electrochemical sensors for melatonin detection. Reproducibility, detection range, and limit of detection are also important concerns. Therefore, a novel anti-fouling and selective electrode

✉ Kamonwad Ngamchuea
kamonwad@g.sut.ac.th

[1] School of Chemistry, Institute of Science, Suranaree University of Technology, 111 University Avenue, Suranaree, Muang, Nakhon Ratchasima 30000, Thailand

[2] Institute of Research and Development, Suranaree University of Technology, 111 University Avenue, Suranaree, Muang, Nakhon Ratchasima 30000, Thailand

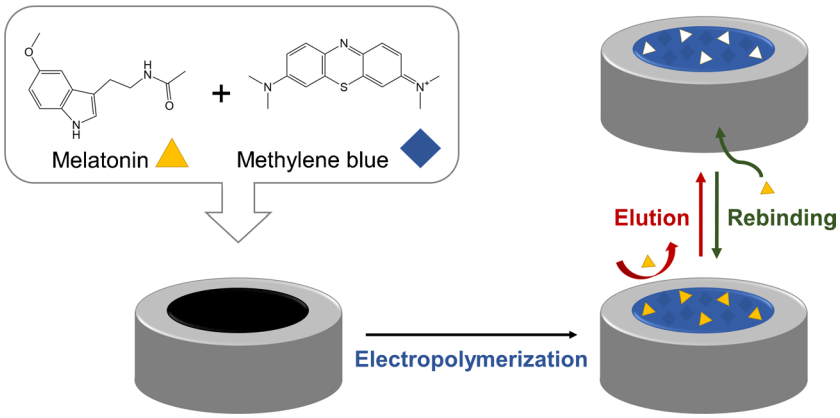

Scheme 1 Preparation of methylene blue molecularly imprinted polymer for melatonin analysis

material is key to developing a durable and accurate electrochemical sensor for melatonin detection.

Recently, functional materials have been utilized to overcome the limitations of traditional electrodes. Among these materials, molecularly imprinted polymers (MIPs) have shown great promise. MIPs are three-dimensional, crosslinked polymers with specific molecular recognition abilities. They are synthesized through polymerization of functional monomer(s) and a template molecule, followed by the removal of the template to create cavities with size, shape, and functional groups specific for interacting with the target analyte through bonding or non-bonding interactions [28, 29].

In this work, we prepared a new porous MIP material by electropolymerizing methylene blue with melatonin as the imprinted template molecule for fast and simple detection of melatonin in urine and saliva samples (Scheme 1). Methylene blue, a widely accessible and cost-effective compound, serves as an ideal candidate for MIP synthesis. It forms a highly electrically conductive polymer, and its electrochemical properties can be adjusted to optimize the detection of melatonin. During the electropolymerization process, the positively charged methylene blue can establish strong electrostatic attractions with the negatively charged melatonin (under neutral conditions). Additionally, methylene blue possesses aromatic rings that can participate in π-π stacking interactions with the aromatic rings in melatonin. These interactions facilitate the creation of well-defined binding sites within the MIP, thereby enhancing the sensor's sensitivity and selectivity towards melatonin.

Experimental

Chemical reagents

All reagents were of analytical grades and used as received without further purification: melatonin ($C_{13}H_{16}N_2O_2$, 99.1%, Supelco), methylene blue ($C_{16}H_{18}ClN_3S.H_2O$, ≥ 99.0%, Qrëc), ethyl alcohol (C_2H_6O, 99.9%, Qrëc), acetic acid glacial (CH_3COOH, 99.8%, Qrëc), potassium chloride (KCl, ≥ 99.0%, Sigma-Aldrich), potassium hexacyanoferrate (II) trihydrate ($K_4[Fe(CN)_6]$ $3H_2O$, ≥ 98.5%, Sigma-Aldrich), potassium hexacyanoferrate (III) ($K_3[Fe(CN)_6]$, ≥ 99.0%, Sigma-Aldrich), sodium hydrogen carbonate ($NaHCO_3$, ≥ 99.0%, Qrëc), sodium carbonate (Na_2CO_3, 99.5%, KemAus), sodium dihydrogen phosphate dihydrate (NaH_2PO_4 $2H_2O$, ≥ 99%, Qrëc), disodium hydrogen phosphate anhydrous (Na_2HPO_4, 99.0%, Qrëc), sodium citrate tribasic ($C_6H_5Na_3O_7$, ≥ 99.0%, Sigma-Aldrich), citric acid anhydrous ($C_6H_8O_7$, 99.5%, Qrëc), serotonin ($C_{10}H_{12}N_2O$, ≥ 98%, Supelco), L-tryptophan ($C_{11}H_{12}N_2O_2$, > 98.5%, TCI), cytosine ($C_4H_5N_3O$, > 98%, TCI), cytidine ($C_9H_{13}N_3O_5$, > 98%, TCI), L-ascorbic acid ($C_6H_8O_6$, ≥ 99.0%, Sigma-Aldrich), creatinine ($C_4H_7N_3O$, ≥ 98%, Sigma-Aldrich), sodium L-lactate ($C_3H_5NaO_3$, ≥ 99.0%, Sigma-Aldrich), urea (CH_4N_2O, ≥ 98%, Sigma-Aldrich), sodium sulfate (Na_2SO_4, > 99.5%, Tokyo Chemical Industry), and alumina powder (1.0, 0.3, and 0.05 µm, Buehler, USA). Deionized water (DI) from the Elga Purelab Ultra water purification system (Elga Labwater, UK) was used for all experiments.

Electrochemical studies

All electrochemical experiments were carried out in N_2-saturated aqueous solutions using a PalmSens4 potentiostat (PalmSens, Netherlands) and a standard three-electrode system in a Faraday cage thermostated at 25 °C. A glassy carbon electrode (GCE, 3.0 mm diameter, ItalSens) a silver/silver chloride electrode (Ag/AgCl in saturated KCl, ItalSens), and a platinum sheet were used as working, reference, and counter electrodes, respectively.

Electrode preparation and characterization

The glassy carbon electrode (GCE) was polished using alumina powder (Buehler, USA) with particle sizes of

1.0 µm, 0.3 µm and 0.05 µm on soft lapping pads (Buehler, USA) and rinsed with deionized water prior to use. To prepare the methylene blue molecularly imprinted polymer, the cleaned GCE was subjected to cyclic voltammetry in the potential range between −0.5 V and 1.4 V at a scan rate of 50 mV s^{-1} for 15 cycles in a solution containing 1.0 mM methylene blue (functional monomer), 0.10 mM melatonin (template), and 0.10 M phosphate buffer pH 7.0. Next, the melatonin template was eluted by immersing the electrode in a 4:1 (V/V) ethanol:acetic acid mixture for 8 min under constant stirring at 300 rpm. This forms the methylene blue molecularly imprinted polymer on a glassy carbon electrode (MIP/GCE) for the analysis of melatonin.

The morphology of the molecularly imprinted polymer was probed by a field-emission scanning electron microscope (Zeiss Auriga FESEM/FIB/EDX, 3.00 kV, Carl Zeiss, Oberkochen, Germany). The functional groups of the formed molecularly imprinted polymer were probed by Fourier-transform infrared spectrometer (ATR-FTIR, Tensor 27, Bruker, Germany).

Application to urine and saliva samples

Urine samples were collected from five healthy volunteers at 12:00 p.m., with a volume of ca. 35 mL per person. Saliva samples were collected from five healthy volunteers between 11:00 a.m. and 12:00 p.m. Prior to collection, the volunteers were instructed to abstain from eating and drinking for one hour. The standard method of using Salivettes (Sarstedt Ltd, Nümbrecht) was employed, wherein the volunteers gently chewed on a cotton swab for one minute and the collected saliva was transferred into a sampling tube. The sample was then centrifuged at 1000 × g for 2 min to remove particles or mucus, and subsequently analyzed for melatonin using the developed electrochemical sensor. After collection, the samples were stored in a refrigerator at a temperature of 2–8 °C.

The samples were spiked with 30 µM melatonin, diluted 25-fold with phosphate buffer pH 7.0, and subjected to DPV measurements at a pulse amplitude of 0.175 V, pulse width of 0.05 s, and a scan rate of 10 mV s^{-1}. The obtained results were analyzed and reported as a percentage recovery (the mean value of triplicate measurements ± standard deviation).

This work was conducted with the ethical approval of the Human Research Ethics Office, Institute of Research and Development, Suranaree University of Technology (EC-65–80). The inclusion criteria for subject selection were healthy Thai volunteers of all genders, aged between 18–60 years old, with no chronic diseases or regular medication use in the following disease groups: eye diseases, spinal cord injuries, liver and kidney diseases, and inflammatory bowel diseases.

Results and discussion

First, the electrochemical properties of melatonin were investigated at a bare glassy carbon electrode (GCE). Next, a melatonin-templated methylene blue molecularly imprinted polymer electrode (MIP/GCE) was fabricated by electropolymerization, with the polymerization method optimized for melatonin detection. The resulting electrodes were then characterized for their thickness, surface morphology, surface functional groups, and charge transfer properties. Finally, the developed sensor was tested for its analytical performance and applied for melatonin analysis in urine and saliva samples.

Cyclic voltammetry of melatonin at bare GCE

The electrochemical properties of melatonin were first investigated using cyclic voltammetry at a bare GCE. An oxidation peak was observed at 0.690 V at a scan rate of 10 mV s^{-1} (Fig. 1a). The absence of the backward peak indicated a chemically irreversible nature of the process. Tafel analysis of the oxidative currents was used to investigate electron transfer kinetics of melatonin, according to Eq. 1 [30–33]:

$$\frac{\partial lnI}{\partial E} = \frac{\left(n\prime + \beta_{n\prime+1}\right)F}{RT} \quad (1)$$

where I is the voltammetric current in the range of 15 – 50% of the peak current at the slow scan rate of 10 mV s^{-1}. This current range was chosen in order to eliminate the mass transport effect [34]. E is the potential, F is the Faraday constant (96,485 C mol^{-1}), R is the molar gas constant (8.314 J K^{-1} mol^{-1}), T is the absolute temperature (298 K), n' is the number of electron transfer before the rate determining step (RDS), $\beta_{n\prime+1}$ is the anodic transfer coefficient of the RDS.

The apparent transfer coefficient $\left(n\prime + \beta_{n\prime+1}\right)$ of melatonin oxidation at a glassy carbon electrode was determined to be 0.74 ± 0.01 (Fig. 1a). The results therefore indicated that the first electron transfer was the rate determining step of the reaction.

Next, the effects of scan rates on the voltammetric responses of melatonin were investigated (Fig. 1b). Figure 1c showed that the peak currents increased linearly with square root of scan rates, indicating a diffusion-controlled process. The diffusion coefficient was then determined according to Eq. 2 to be $1.50 \times 10^{-9} \pm 0.03 \times 10^{-9}$ m^2 s^{-1}.

$$I_p = 0.496\sqrt{n\prime + \beta_{n\prime+1}}nFAc^*\sqrt{\frac{F\nu D}{RT}} \quad (2)$$

where I_p is the peak current of melatonin oxidation, n is the total number of electron transfer, υ is the potential scan rate

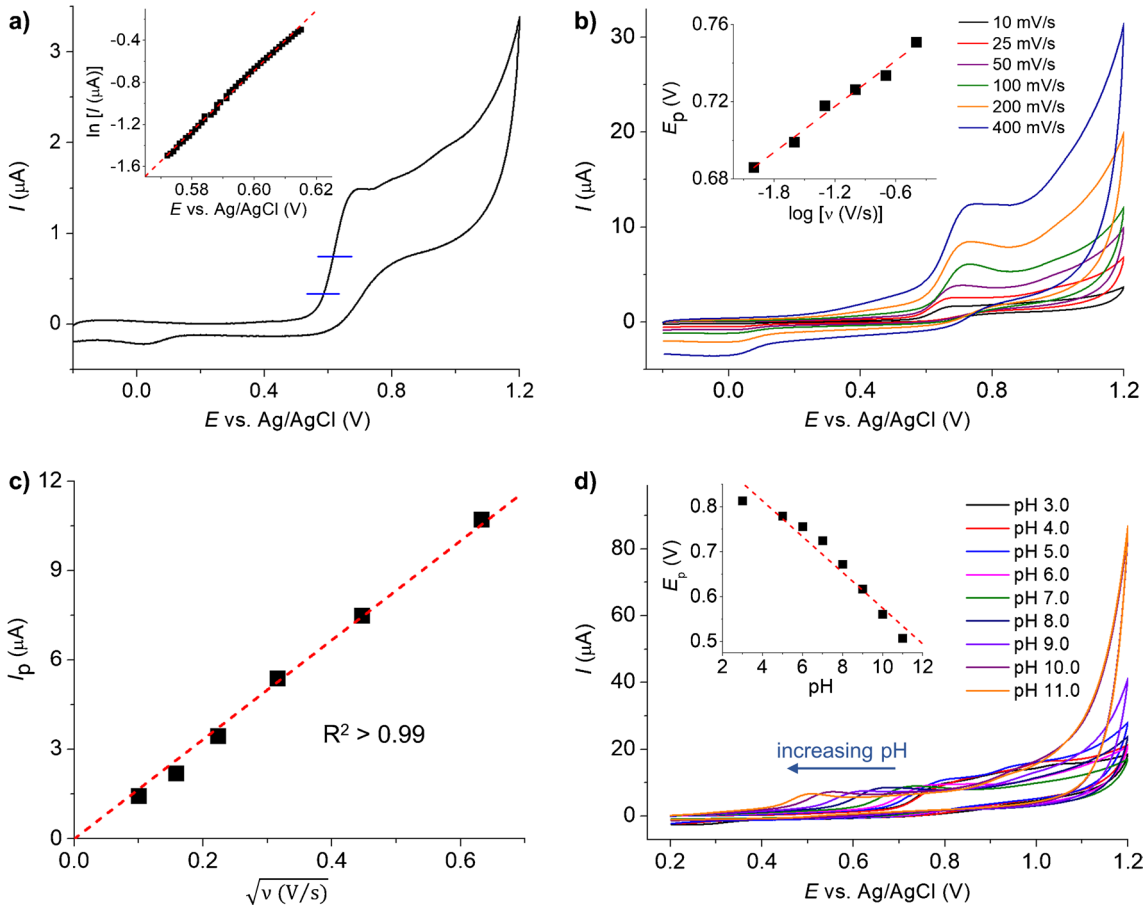

Fig. 1 **a** CV of 200 μM melatonin in phosphate buffer pH 7.0 at a bare GCE at a scan rate of 10 mV s^{-1}. The inlay shows the plot of ln|*I*| vs. *E* in Tafel analysis. **b** CV of 200 μM melatonin at various scan rates (at a bare GCE at pH 7.0). The inlay shows the plot of peak potentials (E_p) vs. log *υ*. **c** The plot of peak currents (I_p) vs. $\sqrt{\upsilon}$. **d** CV of 200 μM melatonin at a bare GCE at various pH

(V s^{-1}), F is the Faraday's constant (96,485 C mol^{-1}), *A* is the electrode surface area (m^2), R is the molar gas constant (8.314 J K^{-1} mol^{-1}), *T* is the absolute temperature (K), and *D* is the diffusion coefficient of the redox active species (m^2 s^{-1}) [35].

The oxidation of melatonin at a bare GCE was next studied under different pH conditions (Fig. 1d). The anodic peaks shifted to lower potentials as the pH increased, indicating of a deprotonation process. The plot of peak potentials (E_p) against pH had the slope of 39.7 ± 3.7 mV pH^{-1}, close to the theoretical value of a process which the number of electrons transferred is double that of protons [36, 37].

According to Eq. 3 and the plot of peak potentials (E_p) against the logarithm of scan rates in the inlay of Fig. 1b, the value of βn was further revealed to be 1.49 ± 0.08. As the value of β was determined to be 0.74 ± 0.01, *n* was therefore ~ 2, indicating that the oxidation melatonin is a $2e^-$ $1H^+$ process, consistent with previous literature reports [36, 37].

$$E_p = \left(\frac{2.303\mathrm{R}T}{\beta n\mathrm{F}}\right)\log(\upsilon) + \left(\frac{2.303\mathrm{R}T}{\beta n\mathrm{F}}\right)\log\left(\frac{\mathrm{R}Tk^0}{\beta n\mathrm{F}}\right) + E^0 \quad (3)$$

where E_p is the peak potential of melatonin oxidation, *n* is the total number of electron transfer, *υ* is the potential scan rate (V s^{-1}), F is the Faraday's constant (96,485 C mol^{-1}), *A* is the electrode surface area (m^2), R is the molar gas constant (8.314 J K^{-1} mol^{-1}), *T* is the absolute temperature (K), and k^0 is the standard electrochemical rate constant, and E^0 is the standard electrode potential.

Preparation and characterization of MIP/GCE

In this section, the molecularly imprinted polymer (MIP) and non-imprinted polymer (NIP) were synthesized by electropolymerization and characterized for their electroactivities, thickness, surface morphology, surface functional groups, and charge transfer properties.

Electropolymerization of MIP

The melatonin-templated methylene blue molecularly imprinted methylene blue polymer (MIP) was formed by successive voltammetry of a stationary GCE in 1.0 mM methylene blue in 0.10 M PBS pH 7.0 buffer in the presence of 0.10 mM melatonin template in the potential range between –0.5 V and 1.4 V at the scan rate of 50 mV s^{-1}. Figure 2a showed that the redox peak currents of methylene blue decreased in successive cycles and gradually reached a constant value after 15 scans, showing continuous formation of the polymer on the electrode surface. The disappearance of the voltammetric responses of the standard redox probe, $[Fe(CN)_6]^{4-}$, at the as-fabricated MIP/GCE in Fig. 2b further evidenced that the electrode surface was covered by the generated polymer.

In the next step, the template was removed from the polymer to create cavities for interacting with the target analyte by eluting the as-fabricated MIP/GCE in 4:1 (V/V) ethanol:acetic acid mixture for 8 min at room temperature under constant stirring at 300 rpm. This step generated a MIP/GCE electrode which was ready for the analysis of melatonin. The successful removal of the template was confirmed by an increase in the response of $[Fe(CN)_6]^{4-}$, indicating that the species could now access the electrode through the cavities in the MIP (Fig. 2b).

The MIP/GCE was then immersed in the solution of 0.10 mM melatonin for 1 min to rebind the electrode with melatonin. Subsequently, the voltammetry of $[Fe(CN)_6]^{4-}$ was performed using the electrode. The resulting voltammogram showed a decrease in peak current, indicating that rebinding of melatonin hindered the access of $[Fe(CN)_6]^{4-}$ through the MIP layer (Fig. 2b).

Thickness of MIP

One of the important factors which determines the analytical performance of the MIP/GCE sensor is the thickness of the polymeric film. The film thickness can be estimated by Eq. 4–6 to be 0.11 µm, 0.19 µm and 0.25 µm after 5, 10 and 15 voltammetric scans in Fig. 2a, respectively [38–40].

$$d = \Gamma V \tag{4}$$

where V is the molecular volume of methylene blue in the polymer ($V = 400\ cm^3\ mol^{-1}$) [41]. Γ is the surface coverage (mol cm^{-2}), which can be calculated by:

$$\Gamma = \frac{Q}{nFA} \tag{5}$$

where n is the number of electrons transferred per molecule of methylene blue ($n = 2$), F is the Faraday's constant (96,485 C mol^{-1}), and A is the surface area of the electrode (cm^2).

Q is the total charge transferred in the electropolymerization process (C):

$$Q = \int I\mathrm{d}t = \frac{1}{\upsilon}\int I\mathrm{d}E \tag{6}$$

where I is the electrical currents during the oxidation of methylene blue in the potential range between –0.2 V and 0.5 V, t is the experimental time, E is the applied potential, and υ is the potential scan rate (V s^{-1}).

Surface morphology

The successful electrodeposition of the methylene blue molecularly imprinted polymer (MIP/GCE) and its surface morphologies were analyzed using SEM imaging and

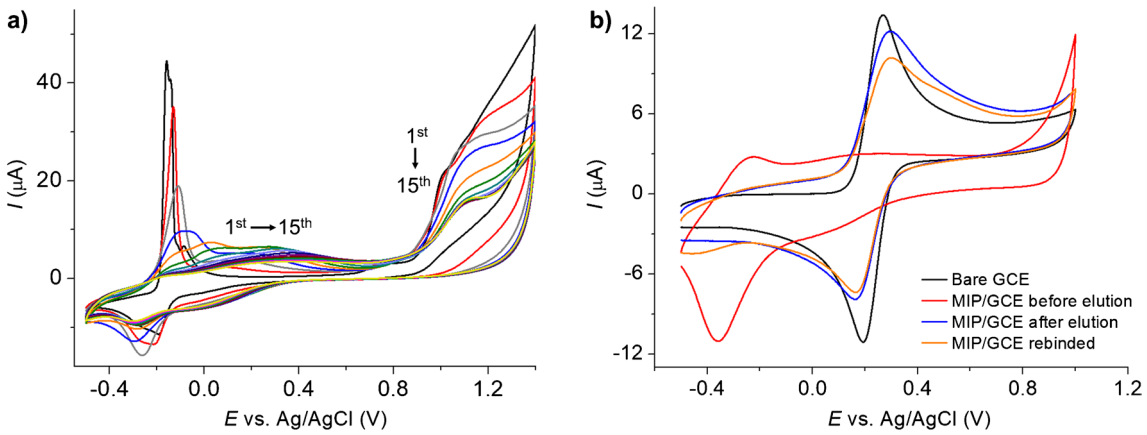

Fig. 2 **a** CV during the electrochemical polymerization of MIP/GCE in 1.0 mM methylene blue, 0.10 mM melatonin, and 0.10 M PBS pH 7.0 at the scan rate of 50 mV s^{-1} for 15 cycles. **b** CV in 1.0 mM $[Fe(CN)_6]^{4-}$ of (black) bare GCE, (red) MIP/GCE before elution, (blue) MIP/GCE after elution (template removal), (orange) MIP/GCE after rebinding in 0.10 mM melatonin

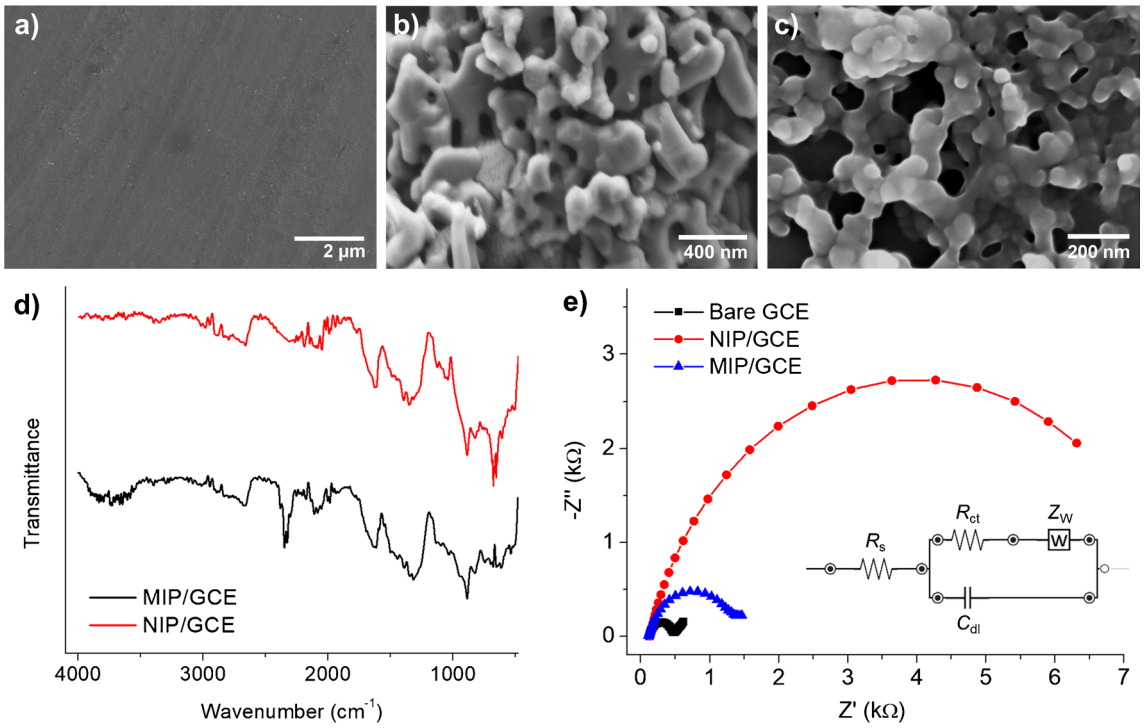

Fig. 3 SEM images of (**a**) bare GCE, (**b**) NIP/GCE and (**c**) MIP/GCE, (**d**) FTIR spectra of NIP/GCE and MIP/GCE, (**e**) EIS spectra of bare GCE, NIP/GCE and MIP/GCE

compared to bare GC and NIP/GCE (Fig. 3a-c). Overall, the MIP and NIP exhibited similar interconnected shapes, but the NIP appeared to be denser. The number and size of cavities in MIP/GCE was found to be higher than those in NIP/GCE. MIP/GCE also showed spherical particles of approximately 55 ± 13 nm in diameter on the interconnected surface.

Surface functional groups

Fourier-transform infrared spectroscopy (FTIR) was used to analyze the surface functional groups of the formed polymers (Fig. 3d). Both MIP/GCE and NIP/GCE showed the peaks at 888 cm^{-1} of C-N stretching, 1321 cm^{-1} of C = S stretching and C-H aromatic bending, and 1633 cm^{-1} of C = C aromatic stretching (IRCalc) [42]. A broad peak at 3500 – 3800 cm^{-1} was additionally observed at MIP/GCE due to the N–H stretching in melatonin, which was used as the template.

Charge transfer properties

Next, the electron transfer at the electrode/solution interface was studied by electrochemical impedance spectroscopy (EIS) in a solution containing 5.0 mM $[Fe(CN)_6]^{3-/4-}$ in 0.10 M KCl over the frequency range of 1 – 10^5 Hz at the amplitude of 5 mV. Figure 3e illustrates the Nyquist plots of bare GCE, NIP/GCE, and MIP/GCE. Randle's equivalent circuit (Fig. 3e, inlay) was used to analyze the EIS spectra, where R_{ct} is the electron transfer resistance, C_{dl} is the double layer capacitance, R_s is the resistance of the electrolyte solution, and Z_W is the Warburg resistance arising from the diffusion process. The double layer capacitances (C_{dl}) were 0.55 µF, 3.11 µF, and 2.94 µF for bare GCE, NIP/GCE, and MIP/GCE, respectively. The values of R_{ct} were determined to be 0.32 kΩ, 2.78 kΩ, and 0.95 kΩ for bare GCE, NIP/GCE, and MIP/GCE, respectively. The lower charge transfer resistance at MIP/GCE as compared to NIP/GCE could be attributed to the presence of the imprinted sites which facilitate the electron transfer at the electrode/solution interface.

The bare GCE, NIP/GCE, and MIP/GCE electrodes were further characterized for their electroactive surface area by cyclic voltammetry of the $[Fe(CN)_6]^{4-}$ redox system at various scan rates. The results can be found in in the supporting information.

Cyclic voltammetry of melatonin at MIP/GCE

The MIP/GCE electrodes were next employed in the detection of melatonin. Figure 4 compared the voltammetric responses of 0.10 mM melatonin in 0.10 M PBS pH 7.0 at MIP/GCE with NIP/GCE and bare GCE. At NIP/GCE and MIP/GCE, the oxidation peak currents of melatonin were enhanced by 2.1-fold and 2.7-fold, respectively, due to the increase in the electroactive surface area. Peak splitting was

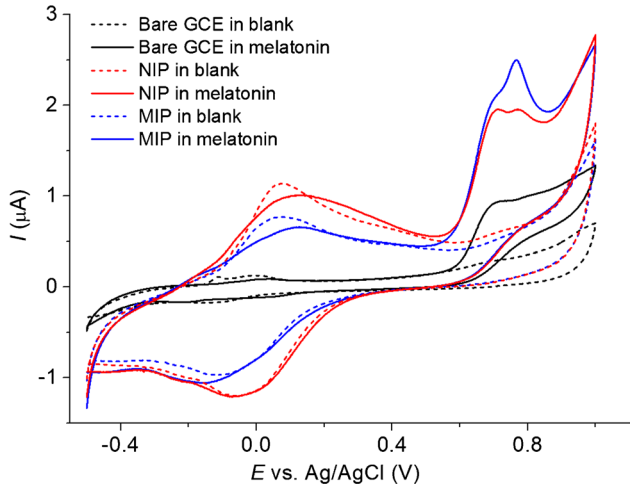

Fig. 4 CV of MIP/GCE vs. NIP/GCE vs. bare GCE in 100 μM melatonin in 0.10 M PBS pH 7.0 at the scan rate of 10 mV $s.^{-1}$

observed at NIP/GCE and MIP/GCE presumably due to the interplay of electrode kinetics and solution-phase mass transport of the electroactive species i.e. thin-layer diffusion inside the pores vs. planar diffusion from bulk solution to the electrode surface, usually observed for electrochemical reactions at porous electrode materials [43, 44].

Optimization of MIP formation conditions

In this section, the parameters which affected the formation and analytical performance of the MIP/GCE sensor were investigated.

Effects of functional monomer concentrations

The concentration of the functional monomer (methylene blue) influences the amount and morphology of the resulting MIP, and hence the sensitivity of the measurement. Figure 5a showed that the responses of melatonin at the MIP/GCE increased with increasing amount of methylene blue, likely due to an increase in the electroactive surface area of the form polymer. When the melatonin template was fixed at 0.10 mM, the concentration of methylene blue which gave the highest current in melatonin detection was 1.0 mM. At higher methylene blue concentrations, the current responses of melatonin decreased, possibly due to slow diffusion of the analyte within the thick polymeric layer [45].

Effects of template to functional monomer ratios

The ratio of functional monomer (methylene blue) to the template (melatonin) plays an important role in determining the size, shape, and selectivity of binding sites in MIPs. If the ratio of template to functional monomer is too low, the MIPs produced may have limited binding capacity and suboptimal selectivity. On the other hand, if the ratio is excessively high, the resulting MIPs may have binding sites that are overly specific and too small, leading to limitations in binding capacity and selectivity for the target molecule. Figure 5b showed that the most effective template to functional monomer ratios for detecting melatonin were 1:5 and 1:10. Consequently, we decided to utilize the 1:10 ratio in this study to reduce the amount of template needed.

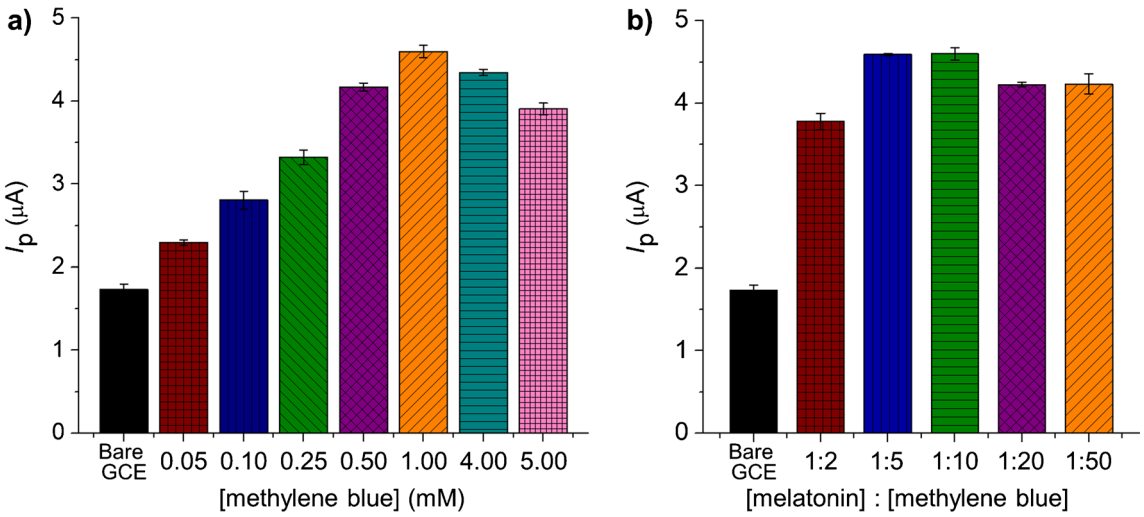

Fig. 5 Peak currents of 100 μM melatonin oxidation at MIP/GCE prepared using (**a**) different concentrations of the methylene blue (functional monomer), (**b**) different ratios of melatonin (template):methylene blue (functional monomer)

Effects of pH during the formation of MIP

The pH of the polymerization environment can affect the chemical interactions between the template (melatonin) and functional monomer (methylene blue), ultimately affecting the quality and selectivity of the resulting MIP. Figure 6 showed that the electropolymerization at higher pH yielded higher current responses in melatonin detection. The current responses at pH 7.0 – 10.0 were not significantly different within the experimental errors of ± 5%. The solution pH of 7.0 was thus chosen for melatonin analysis.

From all the results in Section "Optimization of MIP formation conditions", we can thus concluded that the optimal conditions for the formation of MIP/GCE were 100 µM melatonin and 1.0 mM methylene blue at pH 7.0.

Effects of pH during the analysis of melatonin at MIP/GCE

Figure 7 illustrates the voltammograms of 100 µM melatonin at a MIP/GCE at various pH levels. The oxidation peaks of melatonin shifted to lower overpotentials as the pH of the solution increased by 41.8 ± 1.9 mV pH^{-1}. This shift suggests a $2e^-$ $1H^+$ oxidation of melatonin, which is similar to the observations made at a bare GCE in Sect. 3.1.

Calibration plot: CV

The voltammograms of various concentrations of melatonin at MIP/GCE are demonstrated in Fig. 8. At MIP/GCE, the oxidation peak currents increased linearly with melatonin concentrations in the range of 23.3 – 200 µM with the sensitivity of 40.8 ± 1.5 µA $µM^{-1}$ and the limit of detection ($3S_B/m$) of 0.24 µM (Fig. 7, inlay), significantly better than

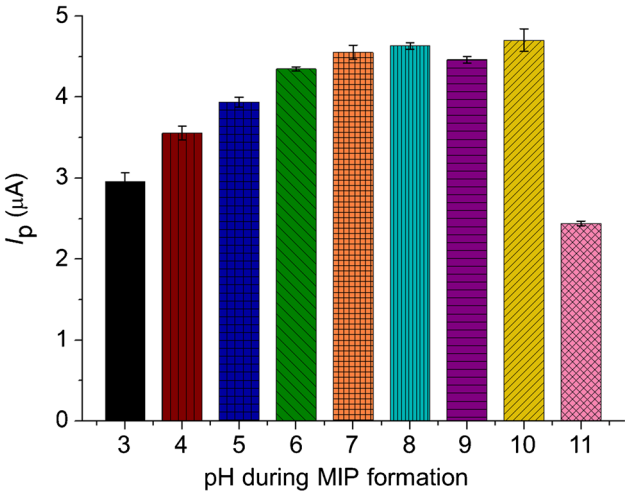

Fig. 6 Peak currents of 100 µM melatonin oxidation at MIP/GCE prepared using different pH during the electropolymerization process

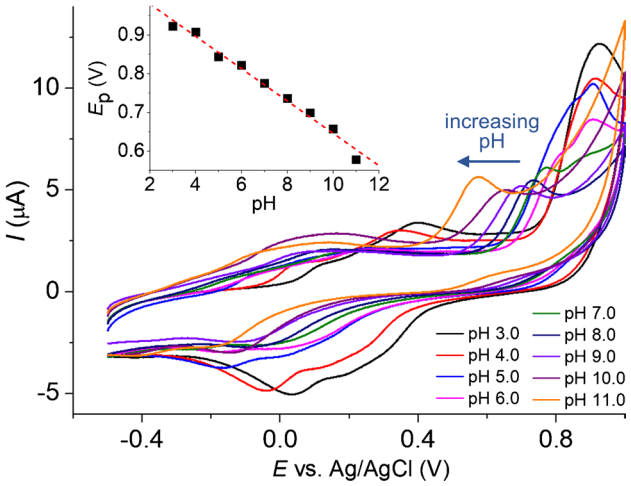

Fig. 7 CV of 100 µM melatonin at various pH at a MIP/GCE at a scan rate of 50 mV s^{-1}. The inlay shows a plot of anodic peak potentials against pH of the solution

a bare GCE (sensitivity of 13.6 ± 0.2 µA $µM^{-1}$ and LOD ($3S_B/m$) of 13.6 µM) and NIP/GCE (sensitivity of 31.8 ± 1.9 µA $µM^{-1}$ and LOD ($3S_B/m$) of 0.30 µM).

Differential pulse voltammetry

The analytical performance of the MIP/GCE was further improved via the use of differential pulse voltammetry (DPV) to eliminate the capacitive background charging currents. The effects of the pulse amplitude (E_{pulse}) towards the analysis of melatonin were investigated in Fig. 9a. As

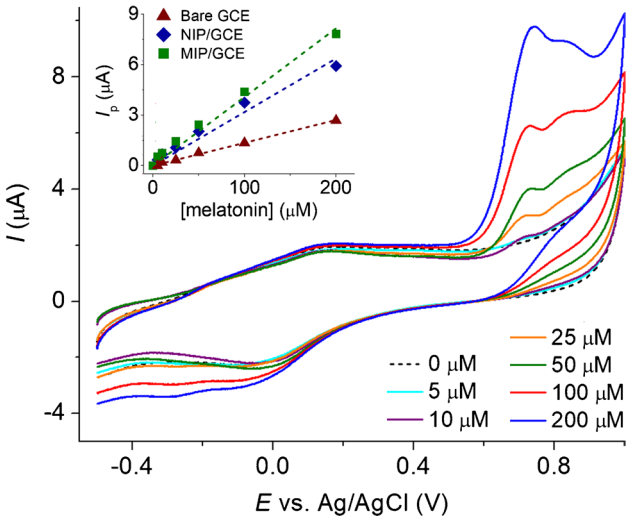

Fig. 8 CV of varied melatonin concentrations in PBS buffer pH 7.0 at a MIP/GCE at a scan rate of 50 mV s^{-1}. The inlay shows the plots of anodic peak currents at MIP/GCE, NIP/GCE and bare GCE against the concentrations of melatonin

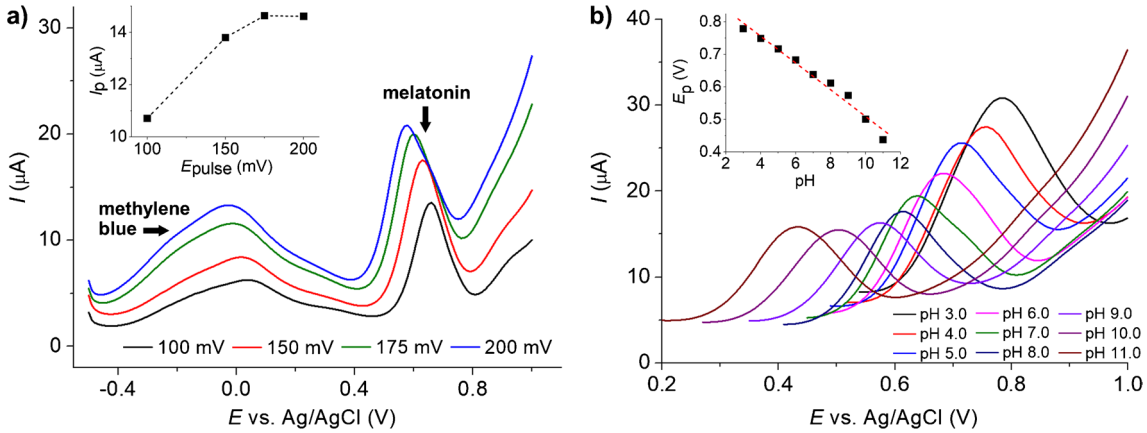

Fig. 9 **a** DPV of 100 μM melatonin in PBS pH 7.0 at different pulse amplitudes (υ = 10 mV s^{-1}, E_{step} = 10 mV, t_{pulse} = 0.05 s); the inlay shows the plot of melatonin oxidation peak currents vs. pulse amplitude. **b** DPV of 100 μM melatonin at various pH (E_{pulse} = 175 mV, υ = 10 mV s^{-1}, E_{step} = 10 mV, t_{pulse} = 0.05 s). The inlay shows the plot of anodic peak currents vs. pH

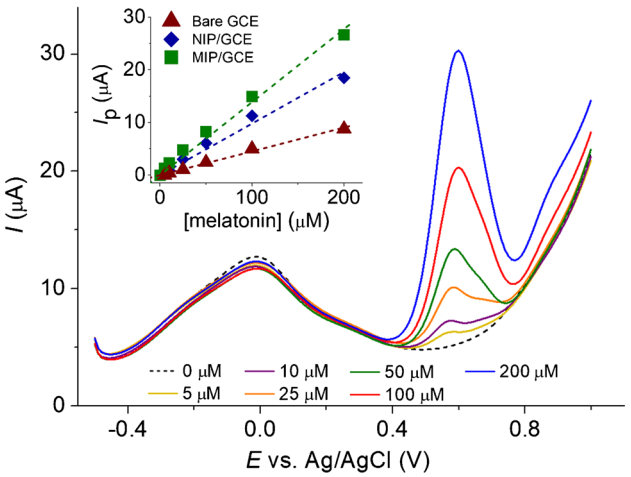

Fig. 10 DPV of different melatonin concentrations in PBS pH 7.0 (E_{pulse} = 175 mV, υ = 10 mV s^{-1}, E_{step} = 10 mV, t_{pulse} = 0.05 s). The inlay shows the plots of anodic peak currents at the potential of 0.60 V vs. Ag/AgCl [saturated KCl] at MIP/GCE, NIP/GCE and bare GCE against the concentrations of melatonin

E_{pulse} increased, the peak currents of melatonin oxidation increased and then reached a maximum at 175 mV. This value of E_{pulse} was thus chosen for the analysis of melatonin.

The effects of pH on the DPV responses of melatonin at MIP/GCE are demonstrated in Fig. 9b. The peak potentials (E_p) shifted to lower values as the pH of the solution increased by 41.0 ± 2.4 mV pH^{-1}, consistent with a $2e^-$ $1H^+$ oxidation of melatonin previously investigated by cyclic voltammetry at bare GCE and MIP/GCE.

Figure 10 demonstrated the DPVs of various concentrations of melatonin. The peak currents at the potential of 0.60 V vs. Ag/AgCl [saturated KCl] increased with melatonin concentrations in the linear range of 0.20 – 200 μM with the sensitivity of 138.8 ± 4.7 μA μM^{-1} and the limit of detection ($3S_B/m$) of 0.061 μM, showing significant improvement from bare GCE (sensitivity of 45.3 ± 1.2 μA μM^{-1} and LOD ($3S_B/m$) of 3.7 μM) and NIP/GCE (sensitivity of 98.0 ± 4.5 μA μM^{-1} and LOD ($3S_B/m$) of 0.087 μM). The comparison of the analytical performance of our newly developed sensor with other non-enzymatic electrochemical sensors for melatonin detection is provided in Table 1.

Repeatability, reproducibility and stability

The reproducibility was tested for both intra-electrode (within electrodes) and inter-electrode (between electrodes) measurements. The DPV measurements at three different MIP/GCEs yielded the relative standard deviations (RSD) of 0.6%, 0.5% and 0.8% (n = 3), for 0.005 mM, 0.025 mM, and 0.20 mM melatonin, respectively, demonstrating excellent reproducibility between electrodes. The RSD values of three DPV measurements at a single MIP/GCE were found to be 1.2%, 0.3% and 2.9% (n = 3) for 0.005 mM, 0.025 mM, and 0.20 mM melatonin, respectively, indicating excellent repeatability within the electrode. The sensitivity of melatonin measurement at a single MIP/GCE was determined to be 131.4 ± 5.3 μA μM^{-1}, which was not significantly different from the sensitivity obtained using the freshly prepared MIP/GCEs (n = 3) of 138.8 ± 4.7 μA μM^{-1}. This finding confirms the excellent repeatability of the electrode. However, when the MIP/GCE was stored under atmospheric conditions at room temperature, its response dropped to 82% of the initial response after 1 day. Subsequently, the response remained at 81.0 ± 1.4% of the initial response for at least 7 days. These results suggest that the MIP/GCE should either be prepared fresh for optimal performance or be used at approximately 80% efficiency for one week.

Table 1 Comparison of non-enzymatic electrochemical sensors for melatonin detection

Electrode	Technique	Linear range (μM)	Detection limit (μM)	Ref
4-AMP/PEDOT/GCE	LSV	0 – 100	0.171	[46]
Acetylene black/Chitosan/Au	SWV	20 – 450	1.9	[47]
Fe_3O_4 NP/rGO/CPE	SWV	0.02– 5.80	0.0084	[48]
GR/AHNSA/MM/GCE	SWV	0.05 − 100	0.0060	[49]
NAD/GI EDTA-WO_3/GCE	SWV	0.010 – 1000	0.0026	[50]
ZnO nanorods/CPE	SWV	0.3 – 100	750	[51]
AuNP–MoS_2 nanoflake/GCE	DPV	0.033 – 10.0	0.0157	[52]
FeCo@CNFs/GCE	DPV	0.08– 400	0.0027	[53]
CNT/SPE	DPV	5 – 3000	1.1	[54]
CuO–poly(l-lysine)/GR	DPV	0.016 μ – 1110	0.016	[55]
PdNP carbon aerogel	DPV	0.02 – 500	0.0071	[56]
SnO_2-Co_3O_4@rGO/CPE	DPV	0.02 – 6.00	0.0041	[57]
Zinc ferrite NP/CPE	DPV	6.5 – 145	3	[58]
MB-MIP/GCE	DPV	0.20 – 200	0.061	This work

Abbreviations: *AHNSA* 4-amino-3-hydroxy-1-naphthalenesulfonic acid, *4-AMP* 4-aminothiophenol, *CNFs* carbon nanofibers, *CNT* carbon nanotube, *CPE* carbon paste electrode, *DPV* differential pulse voltammetry, *GCE* glassy carbon electrode, *GR* graphene, *LSV* linear sweep voltammetry, *MB* methylene blue, *MIP* molecularly imprinted polymer, *MM* melamine, *NAD/GI EDTA-WO$_3$* nicotinamide adenine dinucleotide immobilized gamma ray irradiated ethylene diamine tetraacetic acid-tungsten trioxide, *NP* nanoparticle, *PEDOT* poly(3,4-ethylenedioxythiophene), *rGO* reduced graphene oxide, *SPE* screen printed electrode (carbon), *SWV* square wave voltammetry

Interference studies

The selectivity of the MIP/GCE sensor for melatonin detection was evaluated in Fig. 11 by testing it against potential interferences such as serotonin, tryptophan, lactate, cytosine, cytidine, urea, ascorbic acid, creatine, and creatinine, all of which can coexist with melatonin in urine and saliva samples [59–62]. The results demonstrated that the MIP/GCE sensor exhibited good selectivity against serotonin and tryptophan, with the responses of melatonin unaffected by the concentrations of these species up to twofold and 0.5-fold of melatonin, respectively. The developed MIP/GCE sensor also demonstrated particularly high selectivity against lactate, cytosine, cytidine, urea, ascorbic acid, creatine, and creatinine, and that the concentration of these species up to 100-fold of melatonin had no effect on the melatonin responses (within ± 5% of experimental error). The MIP/GCE's selectivity for melatonin can be attributed to the strong interaction between melatonin and the methylene blue polymer, along with the appropriate host–guest molecular size and interaction.

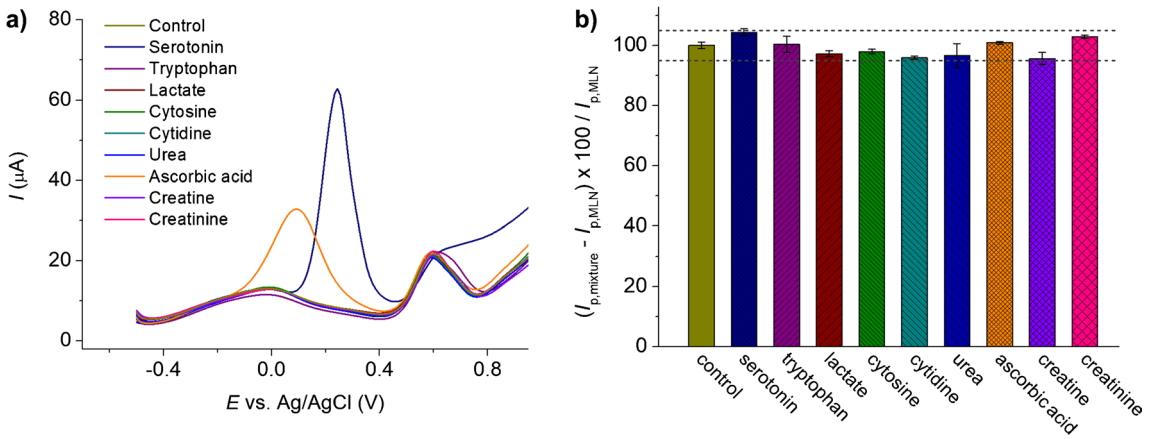

Fig. 11 **a** DPVs (E_{pulse} = 175 mV, υ = 10 mV s^{-1}, E_{step} = 10 mV, t_{pulse} = 0.05 s) and **b** the effects on the peak currents of 100 μM melatonin oxidation in the presence of 200 μM serotonin, 50.0 μM tryptophan, 10.0 mM lactate, 10.0 mM cytosine, 10.0 mM cytidine, 10.0 mM urea, 10.0 mM ascorbic acid, 10.0 mM creatine and 10.0 mM creatinine

While the responses of melatonin were not affected by the tested interferences, it is important to note that matrix interferences, including factors such as sample viscosity, can impact the electrochemical responses. Therefore, it is advisable to employ internal calibration such as standard addition method to enhance the accuracy of melatonin measurements.

Application in urine and saliva samples

The developed MIP/GCE sensor was validated in urine and saliva samples following the method described in Sect. 2.4. The samples were spiked with 30 µM melatonin, diluted 25-fold in PBS buffer pH 7.0, and subjected to DPV measurements ($E_{pulse} = 175$ mV, $\upsilon = 10$ mV s^{-1}, $E_{step} = 10$ mV, $t_{pulse} = 0.05$ s). The percentage recoveries obtained were $103 \pm 1\%$ and $102 \pm 1\%$ for urine and saliva samples, respectively, demonstrating that the sensor can be applied for the analysis of melatonin in these media.

One of the main challenges associated with our approach is the difficulty in controlling the formation of the molecularly imprinted polymer (MIP). The lack of precise control over MIP formation can result in heterogeneity in the imprinting sites, leading to reduced sensitivity in the measurements. Moreover, it is crucial to ensure the complete elution of any residual melatonin before reusing the MIP electrode. Additionally, there is a risk of deformation or damage to the MIP binding sites with repeated use or during long storage periods. Furthermore, several aspects of the imprinting events remain not fully understood, necessitating further enhancements in computational simulation and MIP design. As a result, the development of MIP-based sensors typically entails conducting numerous optimization experiments.

Despite these challenges, our MIP sensor offers several advantages. It features simple operation, utilizes an inexpensive and portable instrument, provides fast analysis times, and offers cost-effective solutions. The sensor exhibits excellent reusability and biomimetic properties. The electrode modification using low-cost methylene blue material through a simple electropolymerization method is also straightforward. These favorable attributes collectively make our sensor a promising and reliable technique for detecting melatonin in biological fluids.

Conclusions

A fast and highly sensitive electrochemical sensor was developed for melatonin detection using a molecularly imprinted polymer (MIP/GCE) with methylene blue as the functional monomer and melatonin as the template. The MIP synthesis involved a simple and low-cost electropolymerization process without the need for initiating reagents. The sensor demonstrated good sensitivity and selectivity due to the large surface area, abundant imprinted sites, and specific host–guest interaction of the MIP. Despite some limitations, such as difficulties in controlling the MIP formation, the need for electrode cleaning before reuse and relatively short shelf-life, the sensor offers advantages including simplicity, affordability, portability, fast analysis time, reusability, and compatibility with biological fluids. Overall, this sensor shows promise for reliable melatonin detection in biomedical applications.

Supplementary Information The online version contains supplementary material available at https://doi.org/10.1007/s00604-023-05930-9.

Acknowledgements This research has received funding support from (i) Suranaree University of Technology (SUT) and (ii) the NSRF via the Program Management Unit for Human Resources & Institutional Development, Research and Innovation (PMU-B) (grant number B13F660067). This work is also supported by Suranaree University of Technology (SUT), Thailand Science Research and Innovation (TSRI) and National Science, Research and Innovation Fund (NSRF; NRIIS number 179313). Ngamchuea K. acknowledges funding from the Thailand Toray Science Foundation (TTSF) under the Science & Technology Research Grants (STRG).

Data availability The authors declare that the data supporting the findings of this study are available within the paper and its Supplementary Information file. Should any raw data files be needed in another format they are available from the corresponding author upon reasonable request.

Declarations

Competing interest The authors declare no known competing financial interests or personal relationships that could have appeared to influence the work reported in this paper.

References

1. Malpaux B, Migaud M, Tricoire H, Chemineau P (2001) Biology of mammalian photoperiodism and the critical role of the pineal gland and melatonin. J Biol Rhythms 16(4):336–347. https://doi.org/10.1177/074873001129002051
2. Wehr TA (1997) Melatonin and seasonal rhythms. J Biol Rhythms 12(6):518–527. https://doi.org/10.1177/074873049701200605
3. Guerrero JM, Reiter RJ (2002) Melatonin-immune system relationships. Curr Top Med Chem 2(2):167–179. https://doi.org/10.2174/1568026023394335
4. Tosini G, Baba K, Hwang CK, Iuvone PM (2012) Melatonin: an underappreciated player in retinal physiology and pathophysiology. Exp Eye Res 103:82–89. https://doi.org/10.1016/j.exer.2012.08.009
5. Yu X, Li Z, Zheng H, Ho J, Chan MT, Wu WKK (2017) Protective roles of melatonin in central nervous system diseases by regulation of neural stem cells. Cell Prolif 50(2):e12323. https://doi.org/10.1111/cpr.12323
6. Doğanlar O, Doğanlar ZB, Delen E, Doğan A (2021) The role of melatonin in angio-miR-associated inhibition of tumorigenesis and invasion in human glioblastoma tumour spheroids. Tissue Cell 73:101617. https://doi.org/10.1016/j.tice.2021.101617

7. Reiter RJ, Tan D-x, Osuna C, Gitto E (2000) Actions of melatonin in the reduction of oxidative stress. J Biomed Sci 7(6):444–458. https://doi.org/10.1007/BF02253360
8. Cardinali DP, Srinivasan V, Brzezinski A, Brown GM (2012) Melatonin and its analogs in insomnia and depression. J Pineal Res 52(4):365–375. https://doi.org/10.1111/j.1600-079X.2011.00962.x
9. Srinivasan V, Spence DW, Pandi-Perumal SR, Trakht I, Cardinali DP (2008) Jet lag: therapeutic use of melatonin and possible application of melatonin analogs. Travel Med Infect Dis 6(1–2):17–28. https://doi.org/10.1016/j.tmaid.2007.12.002
10. Buscemi N, Vandermeer B, Pandya R, Hooton N, Tjosvold L, Hartling L, et al(2004) Melatonin for treatment of sleep disorders: summary, AHRQ evidence report summaries, Agency for Healthcare Research and Quality, Rockville, MD
11. Srinivasan V, Pandi-Perumal S, Maestroni G, Esquifino A, Hardeland R, Cardinali D (2005) Role of melatonin in neurodegenerative diseases. Neurotox Res 7:293–318. https://doi.org/10.1007/BF03033887
12. Pappolla M, Bozner P, Soto C, Shao H, Robakis NK, Zagorski M et al (1998) Inhibition of Alzheimer β-fibrillogenesis by melatonin. J Biol Chem 273(13):7185–7188. https://doi.org/10.1074/jbc.273.13.7185
13. Di Bella G, Mascia F, Gualano L, Di Bella L (2013) Melatonin anticancer effects. Int J Mol Sci 14(2):2410–2430. https://doi.org/10.3390/ijms14022410
14. Kocadağlı T, Yılmaz C, Gökmen V (2014) Determination of melatonin and its isomer in foods by liquid chromatography tandem mass spectrometry. Food Chem 153:151–156. https://doi.org/10.1016/j.foodchem.2013.12.036
15. Chau RM, Patel BA (2009) Determination of serotonin, melatonin and metabolites in gastrointestinal tissue using high-performance liquid chromatography with electrochemical detection. Biomed Chromatogr 23(2):175–181. https://doi.org/10.1002/bmc.1100
16. Nunez-Vergara LJ, Squella J, Sturm J, Baez H, Camargo C (2001) Simultaneous determination of melatonin and pyridoxine in tablets by gas chromatography-mass spectrometry. J Pharm Biomed Anal 26(5–6):929–938. https://doi.org/10.1016/S0731-7085(01)00447-2
17. Sastre Toraño J, Pv R-B, Merkus P, Guchelaar HJ (2000) Quantitative determination of melatonin in human plasma and cerebrospinal fluid with high-performance liquid chromatography and fluorescence detection. Biomed Chromatogr 14(5):306–310. https://doi.org/10.1002/1099-0801(200008)14:5%3c306::AID-BMC986%3e3.0.CO;2-7
18. Sorouraddin M-H, Rashidi M-R, Ghorbani-Kalhor E, Asadpour-Zeynali K (2005) Simultaneous spectrofluorimetric and spectrophotometric determination of melatonin and pyridoxine in pharmaceutical preparations by multivariate calibration methods. Il Farmaco 60(5):451–458. https://doi.org/10.1016/j.farmac.2005.03.009
19. Uslu B, Özkan SA, Aboul-Enein HY (2002) Spectrophotometric determination of melatonin and pyridoxine HCL in binary mixture using first derivative of the ratio spectra method. Anal Lett 35(14):2305–2317. https://doi.org/10.1081/AL-120016104
20. Lee M-H, Thomas JL, Chen Y-L, Lin C-F, Tsai H-H, Juang Y-Z et al (2013) Optical sensing of urinary melatonin with molecularly imprinted poly (ethylene-co-vinyl alcohol) coated zinc oxide nanorod arrays. Biosens Bioelectron 47:56–61. https://doi.org/10.1016/j.bios.2013.03.001
21. Chen G, Ding X, Cao Z, Ye J (2000) Determination of melatonin and pyridoxine in pharmaceutical preparations for health-caring purposes by capillary electrophoresis with electrochemical detection. Anal Chim Acta 408(1–2):249–256. https://doi.org/10.1016/S0003-2670(99)00809-0
22. Poboży E, Michalski A, Sotowska-Brochocka J, Trojanowicz M (2005) Determination of melatonin and its precursors and metabolites using capillary electrophoresis with UV and fluorometric detection. J Sep Sci 28(16):2165–2172. https://doi.org/10.1002/jssc.200500095
23. Welp A, Manz B, Peschke E (2010) Development and validation of a high throughput direct radioimmunoassay for the quantitative determination of serum and plasma melatonin (N-acetyl-5-methoxytryptamine) in mice. J Immunol Methods 358(1–2):1–8. https://doi.org/10.1016/j.jim.2010.03.018
24. Kennaway DJ (2019) A critical review of melatonin assays: Past and present. J Pineal Res 67(1):e12572. https://doi.org/10.1111/jpi.12572
25. Kennaway DJ (2020) Measuring melatonin by immunoassay. J Pineal Res 69(1):e12657. https://doi.org/10.1111/jpi.12657
26. Khan ZA, Hong PJ-S, Lee CH, Hong Y (2021) Recent advances in electrochemical and optical sensors for detecting tryptophan and melatonin. Int J Nanomed 16:6861. https://doi.org/10.2147/IJN.S325099
27. Brazaca LC, Bramorski CB, Cancino-Bernardi J, da Silveira C-M, Markus RP, Janegitz BC et al (2018) An antibody-based platform for melatonin quantification. Colloids Surf B 171:94–100. https://doi.org/10.1016/j.colsurfb.2018.07.006
28. BelBruno JJ (2018) Molecularly imprinted polymers. Chem Rev 119(1):94–119
29. Vasapollo G, Sole RD, Mergola L, Lazzoi MR, Scardino A, Scorrano S et al (2011) Molecularly imprinted polymers: present and future prospective. Int J Mol Sci 12(9):5908–5945. https://doi.org/10.1021/acs.chemrev.8b00171
30. Guidelli R, Compton RG, Feliu JM, Gileadi E, Lipkowski J, Schmickler W et al (2014) Defining the transfer coefficient in electrochemistry: An assessment (IUPAC Technical Report). Pure Appl Chem 86(2):245–258. https://doi.org/10.1515/pac-2014-5026
31. Li D, Lin C, Batchelor-McAuley C, Chen L, Compton RG (2018) Tafel analysis in practice. J Electroanal Chem 826:117–124. https://doi.org/10.1016/j.jelechem.2018.08.018
32. Ngamchuea K, Tharat B, Hirunsit P, Suthirakun S (2020) Electrochemical oxidation of resorcinol: mechanistic insights from experimental and computational studies. RSC Adv 10(47):28454–28463. https://doi.org/10.1039/D0RA06111E
33. Rattanaumpa T, Maensiri S, Ngamchuea K (2022) Microporous carbon in the selective electro-oxidation of molecular biomarkers: uric acid, ascorbic acid, and dopamine. RSC Adv 12(29):18709–18721. https://doi.org/10.1039/D2RA03126D
34. Kaewket K, Maensiri S, Ngamchuea K (2020) Adsorptive stripping voltammetry at microporous carbon: Determination and adsorption characteristics of environmental contaminants. Colloids Interface Sci Commun 38:100310. https://doi.org/10.1016/j.colcom.2020.100310
35. Ngamchuea K, Batchelor-McAuley C, Compton RG (2018) Understanding electroanalytical measurements in authentic human saliva leading to the detection of salivary uric acid. Sens Actuators B Chem 262:404–410. https://doi.org/10.1016/j.snb.2018.02.014
36. Xiao-Ping W, Lan Z, Wen-Rong L, Jian-Ping D, Hong-Qing C, Guo-Nan C (2002) Study on the electrochemical behavior of melatonin with an activated electrode. Electroanalysis 14(23):1654–1660. https://doi.org/10.1002/elan.200290007
37. Corujo-Antuña JL, Abad-Villar EM, Fernández-Abedul MT, Costa-Garcíia A (2003) Voltammetric and flow amperometric methods for the determination of melatonin in pharmaceuticals. J Pharm Biomed Anal 31(3):421–9. https://doi.org/10.1016/s0731-7085(02)00349-7
38. Marinho MIC, Cabral MF, Mazo LH (2012) Is the poly (methylene blue)-modified glassy carbon electrode an adequate electrode for the simple detection of thiols and amino acid-based molecules?

J Electroanal Chem 685:8–14. https://doi.org/10.1016/j.jelechem.2012.08.023
39. Phonklam K, Wannapob R, Sriwimol W, Thavarungkul P, Phairatana T (2020) A novel molecularly imprinted polymer PMB/MWCNTs sensor for highly-sensitive cardiac troponin T detection. Sens Actuators B Chem 308:127630. https://doi.org/10.1016/j.snb.2019.127630
40. Schlereth DD, Karyakin AA (1995) Electropolymerization of phenothiazine, phenoxazine and phenazine derivatives: characterization of the polymers by UV-visible difference spectroelectrochemistry and Fourier transform IR spectroscopy. J Electroanal Chem 395(1–2):221–232. https://doi.org/10.1016/0022-0728(95)04127-A
41. Tan L, Xie Q, Yao S (2004) Electrochemical and spectroelectrochemical studies on pyridoxine hydrochloride using a poly (methylene blue) modified electrode. Electroanalysis 16(19):1592–1597. https://doi.org/10.1002/elan.200302993
42. Jablonka KM, Patiny L, Smit B (2022) Making molecules vibrate: Interactive web environment for the teaching of infrared spectroscopy. J Chem Educ 99(2):561–569. https://doi.org/10.1021/acs.jchemed.1c01101
43. Chen M, Meng Y, Zhang W, Zhou J, Xie J, Diao G (2013) β-Cyclodextrin polymer functionalized reduced-graphene oxide: Application for electrochemical determination imidacloprid. Electrochim Acta 108:1–9. https://doi.org/10.1016/j.electacta.2013.06.050
44. Kaewket K, Ngamchuea K (2023) Microporous carbon for fast and simple electrochemical detection of imidacloprid insecticide in fruit and water samples. RSC Adv 13(7):4532–4541. https://doi.org/10.1039/D3RA00192J
45. Jankhunthod S, Moonla C, Watwiangkham A, Suthirakun S, Siritanon T, Wannapaiboon S et al (2021) Understanding electrochemical and structural properties of copper hexacyanoferrate: application in hydrogen peroxide analysis. Electrochim Acta 394:139147. https://doi.org/10.1016/j.electacta.2021.139147
46. Sun B, Sun W, Wang Z, Zhao B, Yang S (2023) Highly sensitive electrochemical detection of melatonin based on graphene-assisted molecular imprinting technology. Carbon Lett. https://doi.org/10.1007/s42823-023-00504-4
47. Thomas A, Kumar KG (2019) Acetylene black-chitosan mediated electro-oxidation of serotonin and melatonin: an efficient platform for simultaneous voltammetric sensing. Ionics 25:2337–2349. https://doi.org/10.1007/s11581-018-2652-x
48. Bagheri H, Afkhami A, Hashemi P, Ghanei M (2015) Simultaneous and sensitive determination of melatonin and dopamine with Fe_3O_4 nanoparticle-decorated reduced graphene oxide modified electrode. RSC Adv 5(28):21659–21669. https://doi.org/10.1016/s0731-7085(02)00349-7
49. Gupta P, Goyal RN (2015) Graphene and Co-polymer composite based molecularly imprinted sensor for ultratrace determination of melatonin in human biological fluids. RSC Adv 5(50):40444–40454. https://doi.org/10.1039/C5RA04942C
50. Anithaa A, Asokan K, Lavanya N, Sekar C (2019) Nicotinamide adenine dinucleotide immobilized tungsten trioxide nanoparticles for simultaneous sensing of norepinephrine, melatonin and nicotine. Biosens Bioelectron 143:111598. https://doi.org/10.1016/j.bios.2019.111598
51. Molaakbari E, Mostafavi A, Beitollahi H (2015) Simultaneous electrochemical determination of dopamine, melatonin, methionine and caffeine. Sens Actuators B Chem 208:195–203. https://doi.org/10.1016/j.snb.2014.10.130
52. Selvam SP, Hansa M, Yun K (2020) Simultaneous differential pulse voltammetric detection of uric acid and melatonin based on a self-assembled Au nanoparticle–MoS_2 nanoflake sensing platform. Sens Actuators B Chem 307:127683. https://doi.org/10.1016/j.snb.2020.127683
53. Duan D, Ding Y, Li L, Ma G (2020) Rapid quantitative detection of melatonin by electrochemical sensor based on carbon nanofibers embedded with FeCo alloy nanoparticles. J Electroanal Chem 873:114422. https://doi.org/10.1016/j.jelechem.2020.114422
54. Gomez FJV, Martín A, Silva MF, Escarpa A (2015) Screen-printed electrodes modified with carbon nanotubes or graphene for simultaneous determination of melatonin and serotonin. Microchim Acta 182:1925–1931. https://doi.org/10.1007/s00604-015-1520-x
55. Liu Y, Li M, Li H, Wang G, Long Y, Li A et al (2019) In situ detection of melatonin and pyridoxine in plants using a CuO–poly (l-lysine)/graphene-based electrochemical sensor. ACS Sustain Chem Eng 7(24):19537–19545. https://doi.org/10.1021/acssuschemeng.9b04609
56. Rajkumar C, Veerakumar P, Chen S-M, Thirumalraj B, Liu S-B (2017) Facile and novel synthesis of palladium nanoparticles supported on a carbon aerogel for ultrasensitive electrochemical sensing of biomolecules. Nanoscale 9(19):6486–6496. https://doi.org/10.1039/C7NR00967D
57. Zeinali H, Bagheri H, Monsef-Khoshhesab Z, Khoshsafar H, Hajian A (2017) Nanomolar simultaneous determination of tryptophan and melatonin by a new ionic liquid carbon paste electrode modified with SnO_2-Co_3O_4@ rGO nanocomposite. Mater Sci Eng C 71:386–394. https://doi.org/10.1016/j.msec.2016.10.020
58. Tavakkoli N, Soltani N, Shahdost-Fard F, Ramezani M, Salavati H, Jalali MR (2018) Simultaneous voltammetric sensing of acetaminophen, epinephrine and melatonin using a carbon paste electrode modified with zinc ferrite nanoparticles. Microchim Acta 185:1–11. https://doi.org/10.1007/s00604-018-3009-x
59. Dalirirad S, Steckl AJ (2020) Lateral flow assay using aptamer-based sensing for on-site detection of dopamine in urine. Anal Biochem 596:113637. https://doi.org/10.1016/j.ab.2020.113637
60. Abellán-Llobregat A, González-Gaitán C, Vidal L, Canals A, Morallon E (2018) Portable electrochemical sensor based on 4-aminobenzoic acid-functionalized herringbone carbon nanotubes for the determination of ascorbic acid and uric acid in human fluids. Biosens Bioelectron 109:123–131. https://doi.org/10.1016/j.bios.2018.02.047
61. Abellán-Llobregat A, Vidal L, Rodríguez-Amaro R, Berenguer-Murcia Á, Canals A, Morallon E (2017) Au-IDA microelectrodes modified with Au-doped graphene oxide for the simultaneous determination of uric acid and ascorbic acid in urine samples. Electrochim Acta 227:275–284. https://doi.org/10.1016/j.electacta.2016.12.132
62. Khan MI, Zhang Q, Wang Y, Saud S, Liu W, Liu S et al (2019) Portable electrophoresis titration chip model for sensing of uric acid in urine and blood by moving reaction boundary. Sens Actuators B Chem 286:9–15. https://doi.org/10.1016/j.snb.2019.01.098